IOPscience iopscience.iop.org

Home Search Collections Journals About Contact us My IOPscience

Raman imaging of semiconductor materials: characterization of static and dynamic properties

This article has been downloaded from IOPscience. Please scroll down to see the full text article.

2004 J. Phys.: Condens. Matter 16 S25

(http://iopscience.iop.org/0953-8984/16/2/004)

View the table of contents for this issue, or go to the journal homepage for more

Download details:
IP Address: 129.252.86.83
The article was downloaded on 28/05/2010 at 07:14

Please note that terms and conditions apply.

INSTITUTE OF PHYSICS PUBLISHING JOURNAL OF PHYSICS: CONDENSED MATTER

J. Phys.: Condens. Matter **16** (2004) S25–S37 PII: S0953-8984(04)66767-1

Raman imaging of semiconductor materials: characterization of static and dynamic properties

S Nakashima

National Institute of Advanced Industrial Science and Technology, 1-1-1, Umezono, Tsukuba, Ibaraki 305-8568, Japan

E-mail: nakashima-s@aist.go.jp

Received 30 July 2003
Published 22 December 2003
Online at stacks.iop.org/JPhysCM/16/S25 (DOI: 10.1088/0953-8984/16/2/004)

Abstract
Micro-Raman imaging has been used extensively for characterizing semiconductors. This paper reviews recent developments in the use of Raman microscopy for studying structural and electronic properties of semiconductor crystals and composites. Some results for recent Raman imaging measurements are outlined and discussed.

1. Introduction

Raman spectroscopy is a key technique for characterizing various materials. It provides information about the vibrational and electronic properties of semiconductors that are sensitive to crystalline quality, microstructure, strain, alloy composition and free carrier density. The Raman microprobe [1] has been used widely to study local structural and electrical properties in semiconductors. Point-by-point Raman mapping systems have recently been developed into Raman imaging systems combined with CCD detectors that allow data to be acquired in a short time. The Raman imaging technique has provided a useful way to characterize crystal growth and processing in the fabrication of semiconductor devices. The spatial resolution of conventional Raman microscopes using visible laser light as an excitation source has reached the sub-micron scale.

Up to now Raman imaging (mapping) has been employed to examine spatial distributions of physical properties in narrow-gap III–V semiconductors, IV–IV semiconductors such as Ge, Si and diamond, wide-band-gap semiconductors including SiC and AlGaN and other semiconductors. The micro-Raman imaging of semiconductors has important advantages for characterizing crystal growth, device fabrication processing and the devices themselves. A recent major subject for Raman imaging is the characterization of stress in composite structures [2–14] and at the interface of hetero-epitaxial films such as epitaxial lateral overgrown GaN films [15–19]. The evaluation of the stress in the interfaces of Si and insulators has attracted the long-term interest of researchers [20–24]. The stress is also produced by

 © 2004 IOP Publishing Ltd Printed in the UK

defects in crystals. The measurement of the stress distribution is important for studies of the stress generation mechanism. Characterization results for defect-induced strains are shown later on.

Spatial distributions of impurity concentration and free carrier concentration have been studied by Raman imaging [15, 25, 26]. The free carrier distribution in heterostructures has also been studied by several researchers [27–29]. Intentionally doped semiconductor wafers often have non-uniform impurity distributions. Micro-Raman spectroscopy has been used to evaluate the uniformity of dopants. The inhomogeneous distribution of impurities has been studied for SiC wafers [30]. Processing such as ion implantation, junction formation and impurity diffusion also provides inhomogeneous impurity distributions that will be one of the main subjects of Raman imaging. The profiles of residual damage in ion-implanted and post-annealed Si crystals have been obtained by Raman imaging [31].

The present paper describes the fundamentals of characterization by Raman imaging and the technical importance of Raman imaging. Some results for recent measurements are also presented.

2. Raman imaging techniques

Micro-Raman imaging techniques are classified into three groups from the viewpoint of the illumination method [32–34]. The first is point-by-point illumination. Two-dimensional mapping is done by sequential translation of the sample stage or by scanning of the laser beam. This method provides the best spatial resolution, but obtaining two-dimensional maps is time consuming. The second method is line illumination [21, 31, 35] in which the laser beam is expanded in one direction by a cylindrical lens placed in front of the microscope. The laser beam simultaneously illuminates all the points in a rectangular region of the samples. In this case, the intensity distribution along the line is not uniform, because the original laser beam has a Gaussian profile. The non-uniform intensity distribution is corrected by normalizing the intensity profile of the scattered light by the Raman intensity at each position of a reference sample measured in advance. The one-dimensional Raman image is recorded by a CCD detector. In an alternative method, which can obtain uniform line illumination, the laser beam is deflected using a vibrating galvanometer mirror.

The third method is global (plane) illumination combined [27, 36] with a tunable spectral filter and a two-dimensional CCD detector. This method needs no laser beam scanning nor sample translation, and a two-dimensional image can be obtained quickly. However, at present, the spectral resolution is not sufficient compared with other methods using a grating spectrometer.

The three-dimensional Raman image requires the depth profiling of physical parameters in addition to the imaging in the lateral direction. Several techniques have been employed for depth profiling, as illustrated in figure 1.

The first uses laser light at different wavelengths for the samples examined. The penetration depth of the excitation laser light varies with its wavelength. The depth profiles of stress [6, 7, 10] and lattice damage in annealed GaAs [37] have been studied using different wavelength excitations. In the deep ultraviolet (DUV) region the optical penetration depth varies from only from a few to some tens of nanometres for Si, Ge, GaN, SiC, etc. This enables the examination of nanoscale thin surface layers of semiconductors [10–14].

Another profiling technique uses a confocal microscope [38–42]. The depth profile is obtained by moving the sample stage vertically. Confocal microscopy improves the depth as well as lateral resolution. However, the spatial resolution of confocal Raman spectroscopy is still on the sub-micron scale.

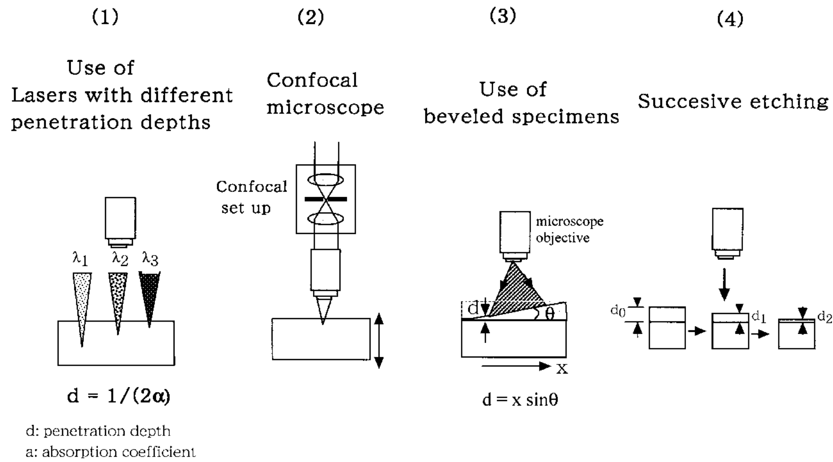

Figure 1. Schematic representation of the methods for obtaining depth profiles.

The third technique uses bevelled specimens combined with line illumination. It has been used to determine the depth profiles of stress [21], carrier density in ZnSe/GaAs interfaces [29] and dopants in GaAs [43, 44]. Since the depth d corresponding to position x in the lateral direction is given by $d = x \sin\theta$, the depth resolution can be improved by using small bevel angle θ.

In the fourth method the depth profile is obtained by successively removing surface layers and performing Raman measurements. This technique has been used to characterize damage in machined silicon layers [45], the amorphous volume fraction in ion-implanted layers [46] and damaged layers in ion-bombarded GaAs [47].

Another method used for obtaining Raman images in the depth direction is cross-sectional measurement of samples with a Raman microscope. Free carrier concentration [15, 25] and local strain [9, 15] have been evaluated.

The spatial resolution of the depth profiling techniques employed so far is generally not sufficient to characterize recent semiconductor heterosystems and devices having fine structures.

3. Results of Raman imaging measurements

3.1. Characterization of crystal growth process

Raman imaging gives us information about not only the spatial distribution of physical quantities but also the dynamical processes such as crystal growth. An interesting example is the result for thermally annealed thin Si films (TSFs) on insulators (SOI) [48]. The Si films were deposited by low-pressure chemical vapour deposition using silane (SiH_4) and disilane (Si_2H_6) as gas sources and were thermally annealed at 600 °C for 5 h. Intensity images of polarized Raman bands were measured on these films using line illumination and translating the sample stage. As shown in figure 2 the intensity profiles exhibited undulation. The undulation may occur because the crystallographic orientation is different for different grains in the film and the grains are tangled at the grain boundaries. In contrast, the intensity profiles of Si films

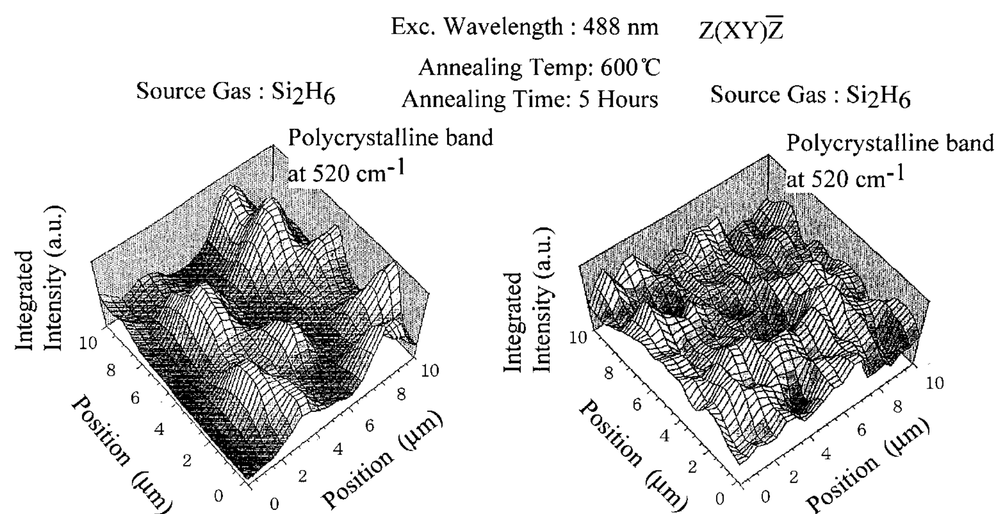

Figure 2. Two-dimensional images of Raman intensity for the Si band at 520 cm^{-1} for films deposited by use of disilane (Si_2H_6) (a) and silane (SiH_4) (b) and post-annealed [48]. The films are annealed at 600 °C for 5 h. The Raman spectra are measured with a polarization configuration.

grown in the liquid phase show an abrupt change at grain boundaries. The estimated average grain size in the disilane–TSF samples is a few microns or larger than that in the silane–TSF samples. The source gas dependence of the grain size is explained by the difference in nucleation rate during the annealing. Since the silane–TSF samples have a large number of nuclei for grain growth, the whole area of the TSF is perfectly crystallized quicker than in the case of disilane–TSF samples, and consequently crystallites in the silane–TSF samples are smaller than those in the disilane–TSF.

3.2. Distribution of stress and carrier density around micropipes

Defects have a strong influence on the structural and electronic properties of semiconductors. Since Raman spectra are sensitive to these properties, they can be used to monitor defects. Micro-Raman imaging is expected to provide novel information about the nature and distribution of the defects. So far, the number of defects induced in the growth process and damage in ion-implanted semiconductors have been evaluated by Raman imaging [31]. In this section we describe Raman imaging of defects in SiC crystals which are wide-gap semiconductors that have attracted much interest due to their potential applications in high-power and high-frequency devices.

SiC crystals often contain defects called micropipes which elongate along the ⟨0001⟩ direction. It is well known that defects of this kind deteriorate the performance of SiC devices. The strains around micropipes have been measured using a polarizing optical microscope and a Raman microscope [50]. We have taken Raman images of strains around micropipes by line illumination. The two-dimensional Raman image is built up by successively moving the sample under the line in 0.5 μm steps. All spectra are carefully fitted to a single Lorentzian line shape and the peak positions are precisely determined. Figure 3(a) shows a polarizing optical microscope photograph in the vicinity of a micropipe. The interference pattern around the micropipe is associated with the distribution of the birefringence formed by internal strain. The Raman frequency images obtained around the micropipe are shown in figure 3(b). The

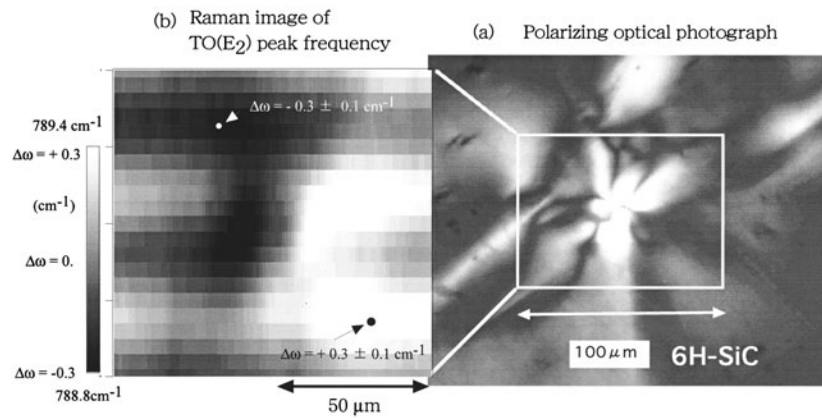

Figure 3. (a) Polarizing optical photograph around a micropipe in 6H-SiC. (b) A two-dimensional image of Raman peak frequency of the TO (E_2) band in 6H-SiC.

frequency difference between the micropipe and the peripheral region is about one-tenth of the wavenumber. The amount of the peak shift due to strain is different for different micropipes. The maximum peak shift for this micropipe is ± 0.3 cm^{-1}. Detecting such a small shift is difficult by point-by-point measurement. The distribution of the strain has no rotational symmetry with respect to the micropipe as shown in this figure. The stress is compressive on one side and tensile on the other side and there are stress-free regions between the strained regions. This strain profile seems to be related to the crystallographic orientations of the sample and the direction of the micropipe. Further studies are required to understand the nature of strains around the micropipes.

Raman images of the longitudinal optical phonon plasmon coupled (LOPC) mode in the vicinity of a micropipe were taken for n-type 4H-SiC crystals with a free carrier concentration of approximately 4×10^{18} cm^{-3} [50]. The laser beam was expanded linearly to 400 μm $\times$ 10 μm on the sample surface, covering the cross-section of the micropipe. Figure 4 shows an image of the LOPC mode. The LOPC Raman band at point A (in the vicinity of the micropipe) lies at a lower frequency than that of other positions. On the other hand, the E_2 (TO) band at 776 cm^{-1} does not show any noticeable change around point A. This result indicates that the crystallinity around the micropipe is almost the same as in the normal region, while the free carrier densities determined by the line shape analysis of the LOPC mode are different, i.e. 3.2×10^{17} cm^{-3} at point A and 1.3×10^{18} cm^{-3} at point B in a micropipe-free region. The most likely explanation is that free carriers are captured by deep traps existing around the micropipe.

3.3. Diodes and modulation-doped specimens

The free carriers density has an inhomogeneous distribution in p–n junction devices and epitaxially grown materials and occasionally in heavily impurity-doped semiconductors. The free carrier concentration can be determined by line shape analysis of the LOPC mode [51, 52]. The carrier concentration and mobility in p–n junctions of GaP diodes have been determined by micro-Raman mapping [53].

Recently, we have obtained Raman images of SiC crystals having a carrier concentration gradient, and examined the doping processes during crystal growth [54]. Samples with the (0001) face were cut from an ingot of 4H-SiC grown by a modified-Lely method in the $\langle 1\bar{1}00 \rangle$ direction. The modulation doping was made by repeated on–off switching of the N_2 gas supply,

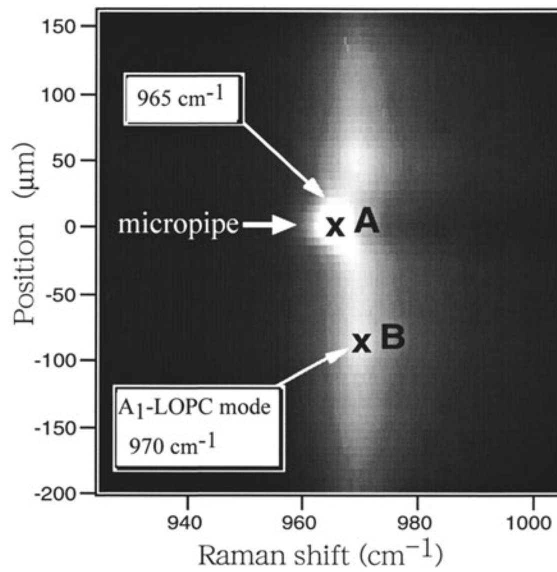

Figure 4. Raman image of LOPC node in n-type 4H-SiC crystal containing micropipes. The micropipe is located at point A. Point B lies in a normal region [50].

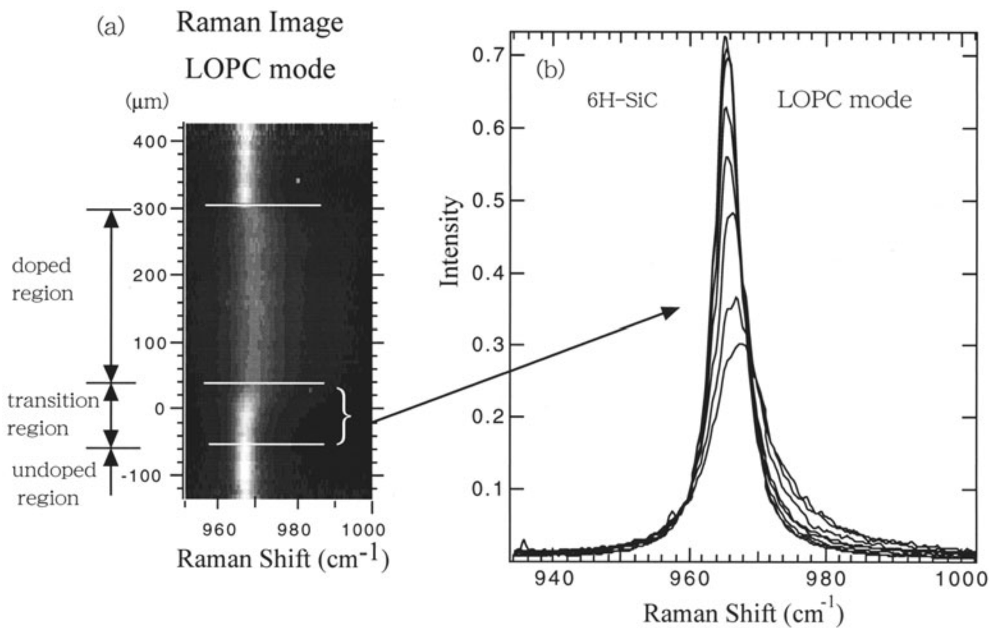

Figure 5. (a) Raman image of the LOPC mode in doped and undoped regions of modulation-doped 6H-SiC. (b) Typical spectra of the LOPC mode in the transition region.

so that the impurity concentration would have a boxcar-type distribution. One-dimensional Raman images of the LOPC mode were obtained at room temperature by line illumination. Figure 5(a) shows a Raman image of the LOPC mode in doped and undoped regions. The peak frequency, intensity and half-width of this mode vary clearly in a transition region between the

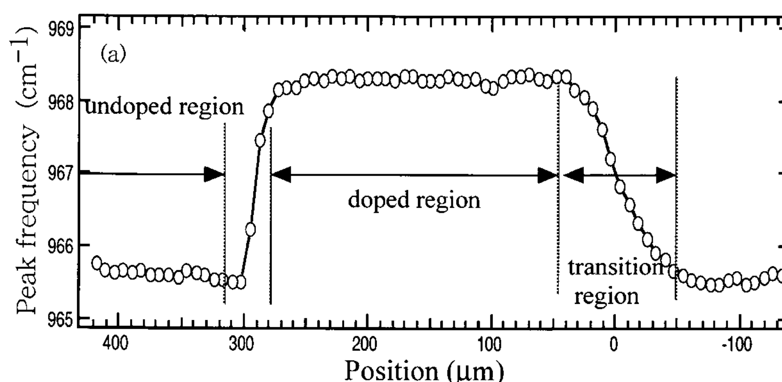

Figure 6. Peak frequency of the LOPC mode in modulation-doped 6H-SiC plotted as a function of the position.

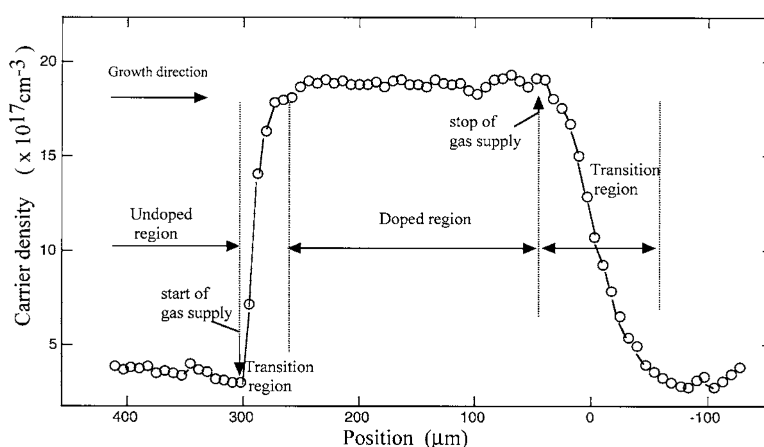

Figure 7. Distribution of the carrier concentration in modulation-doped 6H-SiC.

doped and undoped regions as shown in figure 5(b). The positional dependence of the peak frequency is shown in figure 6. The experimental line shape of the LOPC mode was fitted to the theoretical curve using plasma frequency ω_p, carrier damping γ and LO phonon damping Γ_L as adjustable parameters [55]. The carrier density n and mobility μ were obtained from best fit values of the parameters using the relationship $\omega_p^2 = 4\pi n/(\varepsilon_\infty m^*)$ and $\mu = e/(m^*\gamma)$, where m^* is the carrier effective mass and ε_∞ is the optical dielectric constant.

The carrier (i.e. donor) concentration determined in this way is plotted as a function of distance in figure 7. It rose steeply after doping gas was supplied and decreased slowly after it was stopped. The transition region between the doped and undoped regions is 10–20 μm after the gas supply was tuned on and 70–80 μm after it was turned off. The residual time of the N_2 gas on the surface of the growing crystals inferred from the width of the transition region and the growth rate (about 1 mm h^{-1}) is 250 s, which is longer than the residence time of the N_2 gas in the growth furnace (75 s) which was determined in advance from furnace tests. This result indicates that, after the doping gas was shut off, nitrogen atoms attached to the furnace wall and/or the source were gradually released into the furnace. The relationship between the carrier concentration and mobility is also obtained by this analysis. In the line shape analysis we can now determine the carrier concentration and mobility more accurately

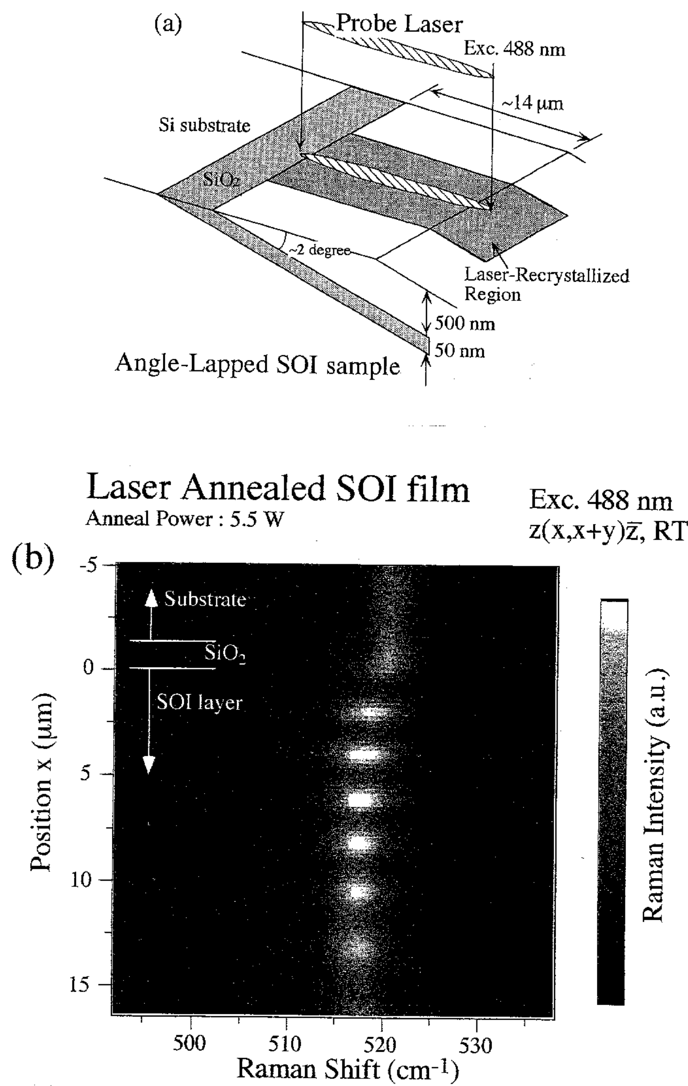

Figure 8. (a) Structure of bevelled SOI. (b) Raman image of the silicon phonon band in recrystallized regions [21].

than before, taking into account that the above parameters vary continuously with position in the sample used in this experiment. Our experimental results demonstrate that the Raman microprobe imaging using samples with a carrier density gradient is useful for characterizing local electrical properties more precisely.

4. Depth profiling

4.1. Bevelled specimens

The resolution of the depth profiling can be improved by using bevelled structures.

Laser-recrystallized silicon films on SiO_2 insulator (SOI) have also been examined by Raman imaging using an angle-lapped specimen [21]. Figure 8(a) schematically shows

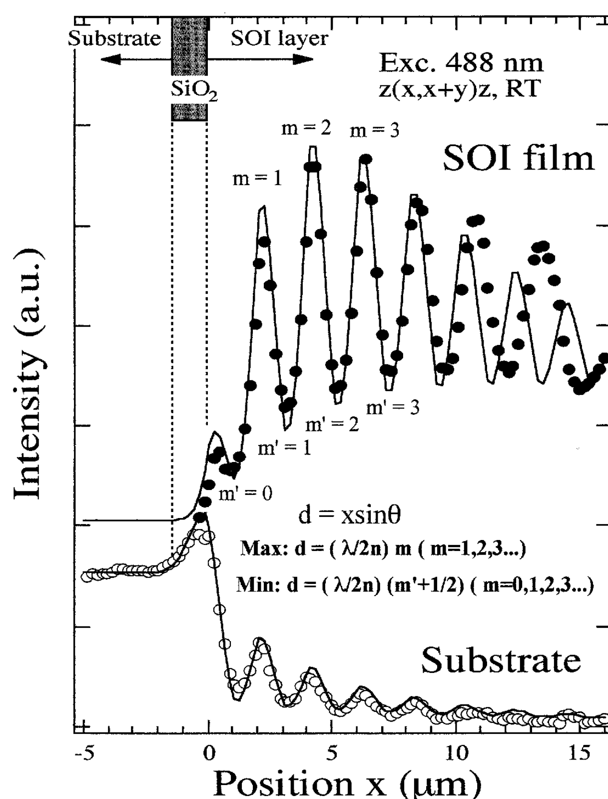

Figure 9. Raman intensity profiles of the Si phonon band in the SOI layer and the substrate. The solid curve shows the calculated profile [21].

the structure of the sample used. The polycrystalline layers were first amorphized by ion implantation and subsequently annealed using a scanning Ar ion laser. Figure 8(b) shows the Raman image of the recrystallized region in the frequency region including the silicon phonon band at 520 cm^{-1}. A periodic variation in the intensity and a slight frequency shift were observed. The intensity profile of the SOI layer is shown in figure 9. The Raman signal from the substrate Si can be separated by Raman polarization measurements and spectral deconvolution. The observed fringe pattern for the Raman intensity arises from multiple reflections and interference effects for the incident and scattered light waves in the recrystallized Si film. The maxima and minima of the fringe pattern appear approximately at $d = m\lambda/2n$ ($m = 1, 2, 3, \ldots$) and $(m + 1/2)\lambda/2n$ ($m = 0, 1, 2, 3, \ldots$), respectively, where n is the refractive index of silicon and λ is the wavelength of the laser light. Note that the Raman intensity enhancement due to interference in the silicon film occurs for both incident and scattered light. This interference effect is useful for obtaining high-precision depth profiles of the films, because the film thickness is precisely determined and Raman signals with a high signal-to-noise ratio are recorded at the high-intensity positions. In fact, the peak frequency and width of the Si phonon band have been determined with a depth resolution of 17 nm [21]. These results indicate that the depth resolution is improved by using bevelled specimens. Figure 10 shows the variation in the bandwidth and peak frequency of the silicon phonon band versus SOI film thickness d. Near the interface region (d = 1–50 nm) the bandwidth increased drastically as d was decreased, whereas the peak frequency did not change much. This result

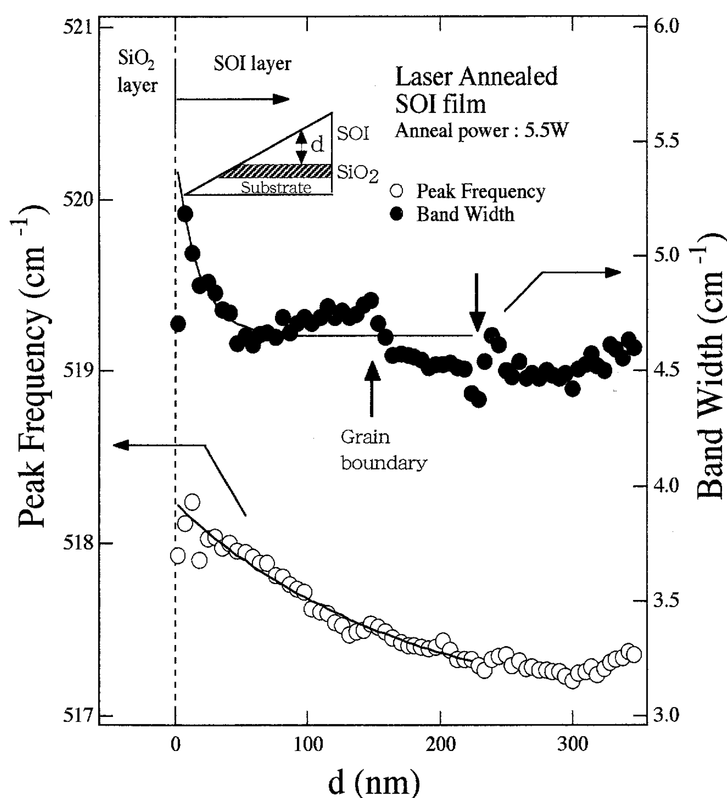

Figure 10. Variation of peak frequency and width of the Raman band as a function of thickness *d* [21].

indicates a high defect density in the interface region between the Si and SiO_2 layers. The variation in the peak frequency suggests that the stress relaxed closer to the interface. The abrupt changes in bandwidth are ascribed to the presence of grain boundaries generated in the SOI film.

4.2. Deep UV Raman microspectroscopy

Wide-gap semiconductors such as SiC and AlGaN are transparent to visible (VIS) light, so Raman measurements of thin surface layers of these materials are difficult with the VIS excitation. We have recently constructed a Raman microspectrometer using deep ultraviolet (DUV) light, which allows us to detect signals from sub-micron thick surface layers of wide-gap semiconductors [14].

Figure 11 compares the Raman spectra for a thin epitaxial layer of SiC taken with DUV (244 nm) and VIS (488 nm) excitations, and a confocal system in the VIS region.

The thickness of the epitaxial layer is 0.5 μm and the free carrier concentration is 5×10^{18} and 5×10^{15} cm^{-3} for the substrate and epitaxial layer, respectively. For VIS excitation the LOPC signals from the substrate appear strongly superimposed on the LO phonon band from the epitaxial layer, while the substrate signal disappears completely for DUV excitation. When a confocal system is used, the Raman intensity of the LO band relative to the LOPC band is increased, but complete removal of the substrate signal is difficult. DUV Raman measurements

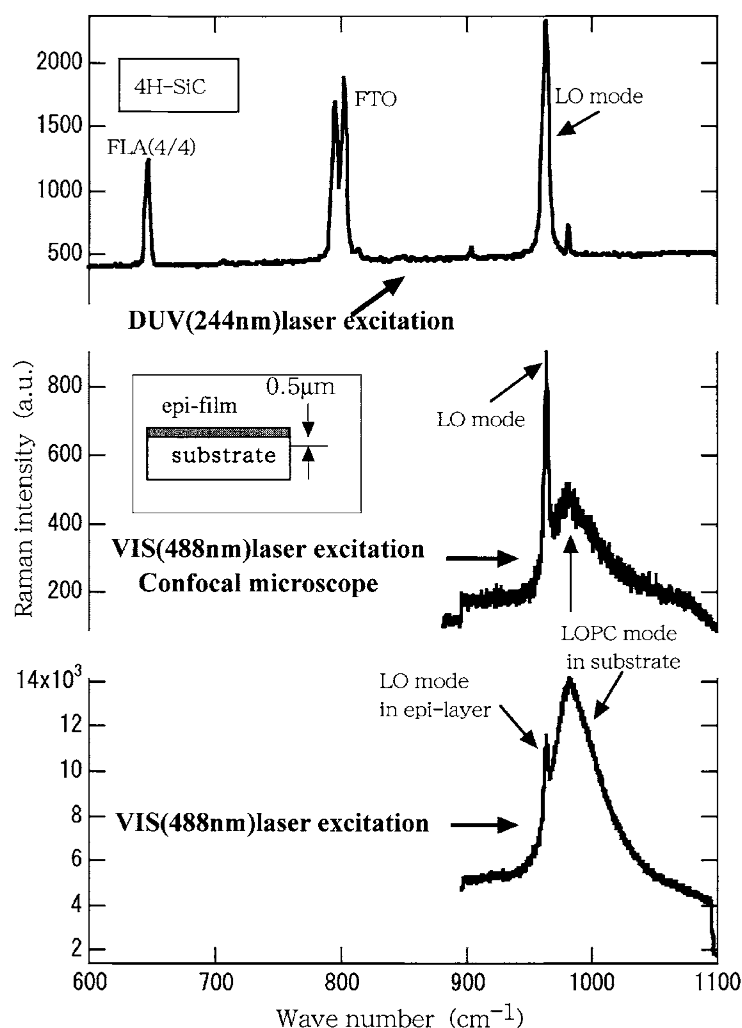

Figure 11. Raman spectra of 0.5 μm thick epitaxial layer of 4H-SiC taken at 244 and 488 nm excitations.

were also carried out for ion-implanted layers of SiC with a projected range of 0.3 μm. The disappearance of signals from the substrate shows that the penetration depth of 244 nm light is less than 0.2 μm for SiC. The above results demonstrate that surface layers of SiC crystals a few hundred nanometres thick can be characterized by the DUV Raman microprobe.

5. Conclusion

Some recent results for the Raman imaging characterization of semiconductors have been described. Raman imaging provides information about not only the spatial distribution of constituents but also the dynamic processes in crystal growth. It is still a growing field, and novel techniques for image measurements and analyses are expected. In the near future this technique should be more widely applied to the study of semiconductor materials.

Acknowledgments

I am grateful to Professor H Harima, Professor K Mizoguchi and Dr T Yamamoto, who made major contributions to the work described in this paper.

References

[1] Turrel G and Corset J (ed) 1996 *Raman Microscopy* (London: Academic)
[2] Schwartz U T, Schuck P J, Mason M D, Grober R D, Roskowski A M, Einfeldt S and Davis R F 2003 *Phys. Rev.* B **67** 045321
[3] Ajito K, Sukamoto P H, Nagahara L A, Hashimoto K and Fujishima A 1995 *J. Vac. Sci. Technol.* A **13** 1234
[4] Rho H, Jackson H E and Weiss B L 1999 *Appl. Phys. Lett.* **75** 1287
[5] Rho H, Jackson H E and Weiss B L 2001 *J. Appl. Phys.* **90** 276
[6] Paillard V, Puech P, Sivin R, Hamma S, Rocai P and Cabarrocas I 2001 *J. Appl. Phys.* **90** 3276
[7] Puech P, Landa G, Carles R, Pizani P S, Daran E and Fontaine C 1995 *J. Appl. Phys.* **77** 1126
[8] Chen H, Li Y K, Peng C S, Liu H F, Liu Y L, Huang Q and Zhou J M 2002 *Phys. Rev.* **65** 233303
[9] Riemann T, Christen J, Kaczmarczyk G, Kaschner A, Hoffmann A, Zeuner A, Hoffmann D and Meyer B K 2002 *Phys. Status Solidi* b **299** 891
[10] Dombrowski K F, De Wolf I and Dietrich B 1999 *Appl. Phys. Lett.* **75** 2450
[11] Dietrich B, Bukalo V V, Fischer A, Dombrowski K F, Bugiel E, Kuck B and Richter H H 2003 *Appl. Phys. Lett.* **82** 1176
[12] Holtz M, Carty J C and Duncan W M 1999 *Appl. Phys. Lett.* **74** 2008
[13] Hortz M, Duncan W M, Zollner S and Liu R 2000 *J. Appl. Phys.* **88** 2523
[14] Nakashima S, Okumura H, Yamamoto T and Shimidzu R 2003 submitted
[15] Tripathy S, Chua S J, Hao M S, Sia E K, Raman A, Zhang J, Sun W H and Wang L S 2002 *J. Appl. Phys.* **91** 5840
[16] Benyoucei M, Kuball M, Beaumont B and Bousquet V 2002 *Appl. Phys. Lett.* **81** 2370
[17] Holtz M, Seon M, Prokofyeva T, Temkin H, Singh R, Davkowski F P and Moustakas T D 1999 *Appl. Phys. Lett.* **75** 1757
[18] Betram F, Riemann T, Christen J, Kaschner A, Hoffmann A, Thomsen C, Hiramatsu K, Shibata T and Sawaki N 2000 *Appl. Phys. Lett.* **74** 359
[19] Kuball M, Benyoucef M, Beaumont B and Gibart P 2001 *J. Appl. Phys.* **90** 3656
[20] Camassel J, Falkovsky L A and Planes N 2000 *Phys. Rev.* B **63** 035309
[21] Mizoguchi K, Nakashima S, Sugiura Y and Harima H 1999 *J. Appl. Phys.* **85** 6758
[22] De Wolf I, Vanhellemont J, Romano-Rodoriguez A, Noström H and Maes E 1992 *J. Appl. Phys.* **71** 898
[23] Yoshikawa M, Maegawa M, Katagiri G and Ishida H 1995 *J. Appl. Phys.* **78** 941
[24] Bonera E, Fanciulli M and Batchelder D N 2002 *Appl. Spectrosc.* **56** 560
[25] Kaschner A, Hoffmann A, Thomsen C, Betram F, Riemann T, Christen J, Hiramatsu K, Sone H and Sawaki N 2000 *Appl. Phys. Lett.* **76** 3418
[26] Matthews M J, Hsu J W P, Gu S and Kuech T 2001 *Appl. Phys. Lett.* **79** 3086
[27] Ponce F A, Steeds J W, Dyer C D and Pitt G D 1996 *Appl. Phys. Lett.* **69** 2650
[28] Araki G, Nittono T, Furuta T and Hyuga F 1998 *Appl. Phys. Lett.* **73** 372
[29] Pagés O, Renucci M A, Briot O and Aulombard R L 1995 *J. Appl. Phys.* **77** 1241
[30] Burton J C, Sun L, Pophristic M, Lukacs S J, Long F J, Feng Z C and Ferguson L T 1998 *J. Appl. Phys.* **84** 6268
[31] Mizoguchi K, Harima H, Nakashima S and Hara T 1995 *J. Appl. Phys.* **77** 3388
[32] Delhaye M and Dahmelincourt P 1975 *J. Raman Spectrosc.* **3** 33
[33] Tread P J and Morris M D 1994 *Appl. Spectrosc. Rev.* **29** 1
[34] Barbillat J 1996 *Raman Microscopy* ed G Turrel and J Corset (London: Academic) chapter 4
[35] Bowden M, Gardiner D J, Rice G and Gerrard D L 1990 *J. Raman Spectrosc.* **21** 37
[36] Markwort L, Kip B, Da Silva E and Roussel B 1995 *Appl. Spectrosc.* **49** 1411
[37] Pizani P S and Campos E M 1998 *J. Appl. Phys.* **84** 6588
[38] Feofanov A, Sharonov S, Valisa P, Da Silva E, Nabiev I and Manfait M 1995 *Rev. Sci. Instrum.* **66** 3146
[39] Kador L, Schittkowski T, Bauer M and Fan Y 2001 *Appl. Opt.* **40** 4965
[40] Matthews M J, Harris A L, Bruce A J and Cardillo M J 2000 *Rev. Sci. Instrum.* **71** 2117
[41] Matthews M J, Hsu J W P, Gu S and Kuech T F 2001 *Appl. Phys. Lett.* **79** 3086
[42] Nishitani-Gamo M, Ando T, Yamamoto K, Watanabe K, Dennig P A, Sato Y and Sekita M 1997 *Appl. Phys. Lett.* **70** 1530

[43] Srnanek R, Gurnik P, Harmatha L and Gregora I 2001 *Appl. Surf. Sci.* **183** 86
[44] Srnaneck R, Kinder P P R, Sciana B, Radziewicz D, MacPhail D S, Littlewood S D and Novotny I 2001 *Appl. Surf. Sci.* **177** 139
[45] Chen L-Q, Zhang X, Zhang T-Y, Lin H Y and Lee S 2000 *J. Mater. Res.* **15** 1441
[46] Holtz M, Zallen R, Brafman O and Matteson S 1988 *Phys. Rev.* **37** 4609
[47] Feng G F, Zallen R, Epp J M and Dillard J G 1991 *Phys. Rev.* B **43** 9678
[48] Mizoguchi K, Yamauchi Y, Harima H, Nakashima S, Ipposhi T and Inoue Y 1995 *J. Appl. Phys.* **78** 3357
[49] Ohsato H, Kato T, Okuda T and Razeghi M 1999 *Proc. SPIE* **3629** 392
[50] Harima H, Hosoda T and Nakashima S 2000 *Mater. Sci. Forum* **338–342** 603
[51] Klein M 1975 *Light Scattering in Solids1* ed M Cardona (Berlin: Springer) p 147
[52] Irmer G, Toporov V V, Bairamov B H and Monecke J 1983 *Phys. Status Solidi* b **119** 595
[53] Nakashima S, Yugami H, Fujii A, Hangyo M and Yamanaka H 1988 *J. Appl. Phys.* **64** 3067
[54] Nakashima S, Nakatake Y, Yano Y, Harima H, Ohtani N and Katsuno M 2002 *Mater. Sci. Forum* **389–393** 633
[55] Harima H, Nakashima S and Uemura T 1995 *J. Appl. Phys.* **78** 1996